Science
AAAS

Supplementary Materials for

Stepwise synaptic plasticity events drive the early phase of memory consolidation

Akihiro Goto *et al.*

Corresponding author: Yasunori Hayashi, yhayashi-tky@umin.ac.jp

Science **374**, 857 (2021)
DOI: 10.1126/science.abj9195

The PDF file includes:

Materials and Methods
Figs. S1 to S10
References

Other Supplementary Material for this manuscript includes the following:

MDAR Reproducibility Checklist

Materials and Methods

Animals.

Animal experiments were conducted in accordance with the guidelines of the Committees for Animal Care of Kyoto University and RIKEN. Mice were housed in groups of one to five per cage with littermates, with a 12 h light/dark cycle and *ad libitum* access to food and water. Mice were single housed post-surgery and throughout the rest of the experiments. All animals were between 10-25 weeks-old, and either wild-type male C57BL/6JJmsSlc mice (WT: SLC) or CaMKIIα-Cre transgenic male mice (Jackson Laboratory; strain Tg (Camk2a-cre) T29-1Stl) (*3*).

Hippocampal slice culture and gene transfection.

Hippocampal organotypic slice cultures were prepared from postnatal day 6-7 rats (*5*). Slices were cultured at 35 ºC on interface membranes (Millipore) and fed with MEM media containing 20% horse serum, 27 mM D-glucose, 6 mM $NaHCO_3$, 2 mM $CaCl_2$, 2 mM $MgSO_4$, 30 mM HEPES, 0.01 % ascorbic acid and 1 μg/ml insulin. pH was adjusted to 7.3 and osmolality to 300-320 mOsm. Slices were biolistically transfected (BioRad) after 5-7 DIV with a plasmid expressing GFP, DsRed2, CFL-GFP, CFL-SN and PAGFP-β-actin under the CAG promoter.

2P microscopy imaging, induction of sLTP in single spines and CALI.

Time-lapse fluorescence imaging was carried out with a 2P microscope (FluoView FV1000MPE, Olympus) equipped with two mode-lock femtosecond-pulse Ti:sapphire lasers (MaiTai HP, Sprectra-Physics). Slices were maintained at room temperature (r.t., 25-27°C) in a continuous perfusion of artificial cerebrospinal fluid (ACSF) containing 119 mM NaCl, 2.5 mM KCl, 3 mM $CaCl_2$, 26.2 mM $NaHCO_3$, 1 mM NaH_2PO_4 and 11 mM glucose, 1 μM tetrodotoxin, 50 μM picrotoxin and 6 mM 4- methoxy-7-nitroindolinyl (MNI)-L-glutamate (Tocris, Bristol, UK) equilibrated with 5% CO_2/95% O_2. A subset of experiments was carried out with 2.5 mM MNI-glutamate and increased (4 mM) $CaCl_2$ concentration. Imaging was performed at 8-9 DIV in primary or secondary dendrites from the distal part of the main apical dendrite of CA1 pyramidal neurons. To avoid overexpression issues, we selected only neurons that had a minimal GFP or DsRed2 signal when excited at 910 nm, but were bright enough to image above noise. Additionally, we ensured that all neurons had typical dendritic morphology and displayed no sign of fluorescent aggregates. Expression of CFL-SN or SN was confirmed at the conclusion of experiments to avoid inadvertent induction of CALI prior to recording, and likewise dendritic morphology was reassessed to confirm neurons remained healthy. sLTP was induced only on thin or small mushroom spines, with a clearly visible head and neck. 2P uncaging of MNI-glutamate was performed using 720 nm light (5 mW), with green and red fluorescence proteins simultaneously excited at 910 nm. Both lasers were aligned daily by imaging and bleaching 0.5 μm fluorescent beads (Invitrogen). sLTP was induced by 1 ms pulses repeated at 1 Hz for 1 min targeted close to the tip of the spine, as previously described (*6*).

For PAGFP experiments, the timing and duration of pulses were as previously explained (*12*). Laser irradiation was focused at a point 0.3–0.5 mm from the tip of a spine and repeated 60 times at 1 Hz with a pulse duration of 0.6 ms. We then collected images of activated PAGFP-actin and DsRed with illumination at 910 nm.

For induction of CALI at 559 nm, a square region (2 μm x 2 μm, 100 pixels x 100 pixels) around the stimulated spine was repeatedly scanned with 559 nm laser (100 μW, LUMPlanFI/IR, 60X/0.90 W, Olympus, 2 μs per pixel dwell time) for 30 sec. For induction of CALI at 593 nm, a laser (YL593T3-030FC, Shanghai Laser & Optics Century Co.) was connected to ferrule with 0.22 NA and a 200-μm-thick protruding cleaved bare optic fiber. The optic fiber was located beside an objective lens for spine imaging and adjusted to focus onto a spot (2 mm in diameter; 0.8 W/cm^2). For the purposes of adjusting the location of fibers, a 473 nm laser (BL473, Shanghai Laser & Optics Century Co.) which does not induce CALI was used, after which it was switched to the 593 nm laser.

Image analysis of sLTP experiments

At every time-point, a series of 512 x 512-pixel XY-scanned images were taken every 1 μm of depth (Z). The fluorescence intensity of 7-10 of these images were summed to obtain a single Z-stack image. A constant region of interest was outlined around the spine including the spine head and half of spine neck and the total integrated fluorescence intensity of the green and red channels was calculated using ImageJ (National Institutes of Health). Values were background-subtracted and corrected for bleed-through and overall fluorescence fluctuations.

Preparation of Adeno-Associated Viruses

pAAV-EF1α-DIO-CFL-SN, pAAV-EF1α-DIO-SN and pAAV-EF1α-DIO-CFL-GFP were constructed by replacing the ChR2-eYFP fusion gene in the pAAV-EF1α-double foxed-hChR2(H134R)-EYFP-WPRE-HGHpA (Addgene plasmid # 20298) with a gene of CFL-SN, SN and CFL-GFP respectively. pAAV-CAG-DIO-CFL-SN-P2A-GCaMP6f was constructed by replacing pAAV-CAG-DIO-ChR2(H134R)-eYFP (Addgene plasmid # 127090) with CFL-SN-P2A-GCaMP6f. GCaMP6f was subcloned from pAAV-CAG-Flex-GCaMP6f-WPRE-SV40 (Addgene plasmid # 100835). To avoid ribosomal read-through, Gly-Ser-Gly was inserted upstream of P2A. We confirmed by western blotting that more than 80% of CFL-SN and GCaMP6f were expressed separately. These plasmids were used to generate AAV vectors. AAV_2-EF1α-DIO-CFL-SN, AAV_2-EF1α-DIO-SN and AAV_9-CAG-DIO-CFL-SN-P2A-GCaMP6f were purified by Iodixanol Gradient Ultracentrifugation (*39)*. The AAV vector used only in Figure 2C (AAV_2-EF1α-DIO-CFL-SN, The AAV_2-EF1a-DIO-SN and AAV_2-EF1a-DIO-CFL-GFP) was purified with a column which binds AAV2 particles (Takara). Viral titer was 1.7 x 10^{13} genome copies (GC) per ml for AAV_2-EF1α-DIO-CFL-SN, 1.9 x 10^{13} GC per ml for AAV_2-EF1α-DIO-SN, 1.2 x 10^{13} GC per ml for AAV_2-EF1a-DIO-CFL-GFP and 5.1 x 10^{13} GC per ml for AAV_9-CAG-DIO-CFL-SN-P2A-GCaMP6f. Among different preparation for the same

virus, viral titer was adjusted by concentrating viral solution with a filter (Millipore). AAV_2-CMV-PI-eGFP-WPRE-bGH was purchased from Penn Vector Core.

Stereotactic Injection and Fiber Optic Implants

Surgical procedures on mice were performed with isoflurane anesthesia, or 500 mg kg^{-1} Avertin (administered intraperitonially and used only in experiments described in Figure 2C). Under stereotaxic guidance, virus was injected using a glass micropipette attached to a microsyringe (MS-10; ITO) through a tube filled with liquid paraffin. 150~500 nl of virus was injected at a rate of 60 nl min^{-1}. Hippocampal CA1 stereotaxic coordinates were -2.3 mm anteroposterior (AP), 1.8 mm mediolateral (ML), and 1.4 mm dorsoventral (DV) from bregma. ACC coordinates were 0.8 mm AP, 0.3 mm ML, 1.2 mm DV. Following viral injection, the needle was held in place for an additional 10 min prior to withdrawal, after which optic fibers were implanted. For CALI, in bilateral hippocampal CA1, mice were implanted with fiber-optic lightguides consisting of a 1.25-mm diameter metal ferrule with 0.5 NA and a 200-µm-thick protruding cleaved bare optic fiber cut to the desired length (Thorlabs) at 0.15 mm dorsal to the injection site. For CALI in bilateral anterior cingulate, dual fiber-optic cannulas of 200 µm thickness and 0.22 NA spaced 0.7 mm apart (Doric Lenses) were lowered 0.2mm above the site of injection. A screw was placed into the skull anterior to the site of injection. A layer of adhesive cement (SHOFU) was applied around the optical fiber. Mice were given 1 mg kg^{-1} Ketoprofen as an analgesic. All viral injection sites were verified at the conclusion of the experiments.

Histology

Mice were transcardially perfused with 4 % paraformaldehyde (PFA) in phosphate buffered saline (PBS). Brains were post-fixed with the same solution for 24 hours, and then sectioned using a vibratome into coronal sections. For immunohistochemistry, the sections were incubated in a buffer (0.1 M Tris-HCl, 0.15 M NaCl) with 0.5 % Triton-X, 5 % blocking reagent (Roche) and primary antibodies and incubated overnight at 4°C. We used rabbit anti-KillerRed antibody (Evrogen, AB961, 1:1000) as a primary antibody to stain SN. After rinsing with PBS 3 times for 15 min each, the sections were subsequently incubated with AlexaFluor 647 conjugated secondary antibodies (Cell Signaling, 1:500) and Hoechst 33258. The sections were then washed with PBS 3 times for 15 min and mounted in VECTASHIELD antifade mounting medium. Fluorescence images were taken with a confocal microscope or with a wide-field fluorescent microscope.

Electrophysiology and CALI.

To express CFL-SN in CA1, a mixture of AAV_2-flox-CFL-SN and AAV2-CMV-PI-eGFP-WPRE-bGH was injected into 8 weeks old CaMKIIα-Cre mice, with the latter being used identify the infected area. Two weeks after injection, all procedures for slice preparation and electrophysiology recording were done under red light to avoid unintended CALI induction. Transverse hippocampal slices (400-µm thickness) were prepared using a McIlwain chopper.

Slices were illuminated with a blue flashlight and inspected for green fluorescence through yellow-colored glasses. Only slices showing green fluorescent in CA1 were used for subsequent recording. Slices were allowed to recover at room temperature for 1.5 h in artificial cerebrospinal fluid (ACSF) and aerated with 95% O_2 and 5% CO_2. Extracellular fEPSPs were recorded with a glass microelectrode (less than 5 Mohm, filled with ACSF) positioned in the *stratum radiatum* of area CA1, while green fluorescence was observed by microscope. A bipolar stimulating electrode was used to elicit fEPSPs every 6 second by stimulation of the Schaffer collateral fibers. A low pass filter (606Hz) was applied to the data and EPSP slope was measured from 10 traces of EPSP during 1 min and averaged. LTP was induced electrically by applying three 1-sec trains (100 Hz) spaced 5 sec apart. After all recordings, expression of CFL-SN (red signal) was confirmed by microscope. EPSP traces in the figures are smoothed using the filter function of MATLAB (Mathworks).
For CALI induction, the samples were exposed to light provided by Hg lamp (BP520-550, 500 μW, 3 min). Optics were adjusted to focus onto a spot (2.3 mm in diameter) on the sample.

Inhibitory avoidance test and CALI.
On the day of the test, mice were briefly anesthetized by isoflurane and optic fibers were connected to deliver 593 nm laser light. After that, the mice were acclimated to the room for at least 20 min in which experiments were to be conducted. The behavioral apparatus used in the experiments was composed of a lit chamber (10 cm (W) x 17 cm (D) x 21 cm (H)) and a dark chamber (20 cm (W) x 17 cm (D) x 21 cm (H)). The lit chamber had a metal grid floor and a white wall without a roof and was illuminated with white light (25k lux). The dark chamber had a metal grid floor and black walls without a roof was illuminated with 940 nm light, which is not visible for mice. The lit chamber was linked to the dark chamber through a sliding door. These chambers were cleaned with 70% ethanol prior to the introduction of each mouse. Mice were placed in a lit chamber for 30 seconds, and the door leading to the dark chamber was then opened. Once the mice had stepped with all four paws into the dark chamber, the door was closed. 20 seconds later, an electric footshock was delivered (0.9 mA, 50 Hz, 3 s, duration of pulse is 1 msec). After the mice were kept in the dark chamber for 1 min, the mice were then returned to their home cage. For memory retention tests, the protocol outlined above was repeated with the exception of the electric shock, and the time latencies for mice to step into the dark chamber was measured. Mice that did not enter the dark chamber within 20 minutes were excluded.
For CALI 1 min, 5min and 10 min after the IA test, mice were returned to home cage immediately after IA testing and kept in the same room until CALI was conducted. Twenty min after CALI (593 nm,1 mW at the fiber tip, 60 sec), mice were briefly anesthetized to detach optic fibers. For CALI 20 min, 60 min, 1 hour and 2 hours after IA testing, optic fibers were connected via a custom rotary joint. After IA test, mice were returned to home cage surrounded by white walls to avoid agitation. Just prior to light illumination for CALI, optic fibers were connected to the 593 nm laser without anesthetic.

For inhibitory avoidance testing during Ca^{2+} imaging, the same procedure explained above was conducted, except mice were placed in a lit chamber for 1 min before door opening and shock was delivered right after mice entered the dark room. For CALI induction through GRIN lens, 593 nm laser was illuminated from an optic fiber (400 μm thickness and 0.53 NA) which was adjusted to be in the focal plane of (500 μm away from) the lens.
For multi-context IA testing, we used two apparatuses with different sizes of box, floor texture, visual cues, color of light and odor. Context-B was a chamber with the same size used for experiment above, with flat plastic floor, visual cues, white color (25k lux) and odor of ethanol in the lit side. Context-A was a chamber (30 cm (W) x 23 cm (D) x 20 cm (H)) with a fluffy floor, another set of distinct visual cues, green color (25k lux) and odor of 0.5% acetic acid in lit side. Context-A was composed of lit and dark chambers of equal size (15 cm (W) x 23 cm (D) x 20 cm (H)).

Polysomnographic recording and CALI

Implantation of electrodes for electroencephalogram (EEG) and electromyogram (EMG) recording was performed as previously described (*21*). Briefly, an EEG screw was implanted over the parietal cortex (7.3 mm AP, 19.5 mm ML) and secured with dental cement. EEG signals were recorded and referenced against a screw implanted in skull over cerebellum. For EMG recordings, a flexible wire cable was implanted into the neck muscle.
Continuous EEG and EMG signals were recorded (Neuralynx), amplified, filtered (EEG, 0.1-50 Hz; EMG, 15–300 Hz), and digitized at a sampling rate of 1 kHz. Both recording wire and optic fibers for CALI were connected to Fiber-optic & Electrical Rotary Joints (Doric), which can transmit both electric current and light, to release the tension from twisting of the wires or cables. For habituation, mice were connected to recording wires at least 4 days prior to recording on a pedestal (22 cm diameter, 30 cm height). The animal's behavior was monitored through a USB camera and recorded on a computer. Recorded data were analyzed by custom-made MATLAB software every 4 seconds. Behavioral states (awake, NREM or REM) were identified by the algorithm previously descried (*21*). Prior to connecting optic fibers from the laser with a ferrule, laser power was adjusted so that final output was 1 mW. Photostimulation was automatically delivered to mice when conditions were met by the computer-based system.

Ca^{2+} imaging.

Ca^{2+} imaging from hippocampus was performed on CaMKIIα-Cre mice two weeks following injection of AAV_9-CAG-DIO-CFL-SN-P2A-GCaMP6f, microendoscope implant, and baseplate surgeries. Imaging was performed in right hippocampus as previously reported (*22, 40*). For habituation, dummy microscopes were mounted on mice, and the mice were housed on a pedestal (22 cm diameter, 30 cm height, termed habituation chamber during Ca^{2+} imaging) in the experimental room at least 4 days prior to recording. On the day of recording, mice were briefly anesthetized to mount the microscope, then returned to the habituation chamber. Twenty min later, recording began, and following a further 2 minutes room lights were turned off. After

further recording for 2 minutes under red light, the IA test was conducted as described above. Ca^{2+} signals from GCaMP6f were imaged during the entire exposure period and were captured at 20 Hz on a miniature microscope (nVista HD, Inscopix). At the conclusion of recording, mice were placed back to home cage and twenty minutes later were anesthetized to detach the microscope. On learning session, the microscope was not mounted and CALI was conducted unilaterally through the lens.

Image processing and cell identification across sessions.

The raw image of each frame was translated into a 16-bit TIFF image and spatially down-sampled (4-pixel bins) with an image decompressor (Inscopix). All subsequent analysis for image processing and cell identification across sessions were conducted by Inscopix Data Processing Software (Inscopix). The images were pre-processed, spatially filtered (low cut-off 0.005 $pixel^{-1}$ and high cut-off 0.5 $pixel^{-1}$), motion-corrected and transformed into $\Delta F/F$ signals. Cells were identified by PCA-ICA [240 output principal components, 200 independent components (ICs), 0.1 weight of temporal information in spatiotemporal ICA, 750 iterations maximum, 1E-5 convergence threshold]. Detected ROIs with >2 components, >70 pixels cell size and <3 SNR (the signal to noise ratio) were excluded from analysis. Ca^{2+} events were detected using the 'Event Detection' function (>4 events threshold factor and >0.4 sec decay time, negative transients were discarded). Across-session neuron registration was performed using the 'Longitudinal Registration' (>0.5 correlation) function.

Selectivity score.

We used the following formula to define the "selectivity score" in each single cell which was commonly active in day 1 and day 2, or day 1 and day 3.

$$\text{Selectivity Score} = (\text{firing rate in lit room} - \text{firing rate in habituation chamber}) / (\text{firing rate in lit room} + \text{firing rate in habituation chamber}).$$

Firing rate in the lit room was defined as the total number of activity events after mice were placed in lit room until 500 frames after the door was opened, divided by time. Firing rate in home cage was defined as the total number of activity events while mice were in the home cage just prior to the IA test, divided by time.

PCA analysis.

PCA was conducted using the MATLAB function 'pca'. PCA was applied to $\Delta F/F$ traces in day 3 concatenated with those from day 1, for each cell which was commonly active on both days (typically 150 cells per mice). Traces on day 1 were captured between the frame when mice were placed in the lit chamber to the frame when mice entered the dark chamber (typically 1200 frames). For Figures 4F-H and 4J, the same length of trace on day 3 was concatenated with it, for

the purposes of PCA analysis. For Figure 4I, traces on day 3 ranged between the frame when mice were placed in the lit chamber and the frame when the mice entered the dark chamber

Synchronous activity.

To identify synchronous activity that included more active cells than would be expected by chance at each frame, we used interval reshuffling (randomly reordering of intervals between events for each cell), performed 1,000 times for each mouse. The threshold percentage of active neurons corresponding to a significance level of $P < 0.05$ was taken to be the per cent of coactive cells required in a single frame to be considered a synchronous event, and this threshold is more than 2.5% active neurons per frame across all mice and fields of view.

Statistical analyses.

Data are expressed as means ± SEM unless otherwise stated. When only two groups were compared, paired two-tailed t tests or two-sided Wilcoxon signed-rank tests were used. When more than two groups were compared, analysis of variance (ANOVA) was used with p values adjusted for *post hoc* multiple comparisons. Significance levels were set to $P=0.05$. Significance is indicated in the figures as follows: *: $P < 0.05$; **: $P < 0.01$. Statistical details including sample sizes and exact p values are described in the figure captions.

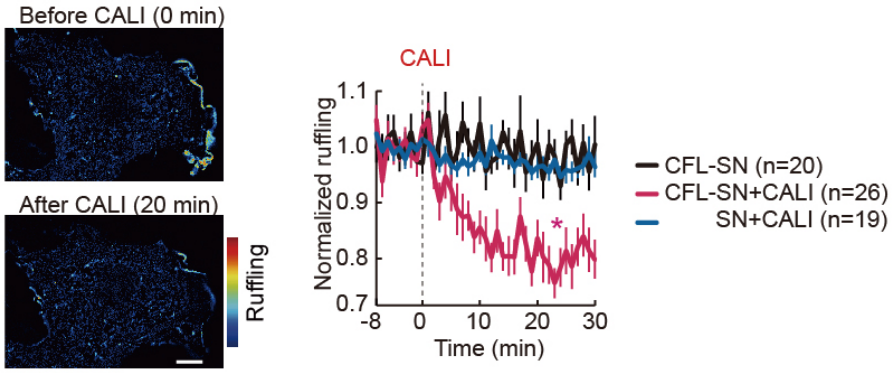

Figure S1. The effect of CALI on actin-dependent movement of lamellipodia.
Actin-dependent movement in lamellipodia of cells expressing GFP-actin is calculated as the change in GFP intensity between 2 successive time points (ruffling) and displayed as pseudocolor (left). Addition to GFP-actin, cells expressed CFL-SN or unfused SN. CALI was induced by scanning whole cells with a 559 nm (100 µW, 2 µs per pixel) laser for 3 min. A graph shows the time course of changes in ruffling, normalized to baseline. Ruffling (20-30 min) was statistically analyzed by a one-way ANOVA test followed by Tukey-Kramer post hoc test. p = 0 (SN+CALI versus CFL-SN+CALI), P=0 (CFL-SN versus CFLSN+CALI), p=0.7047 (CFL-SN versus SN+CALI), $F_{(2,62)} = 33.82$.

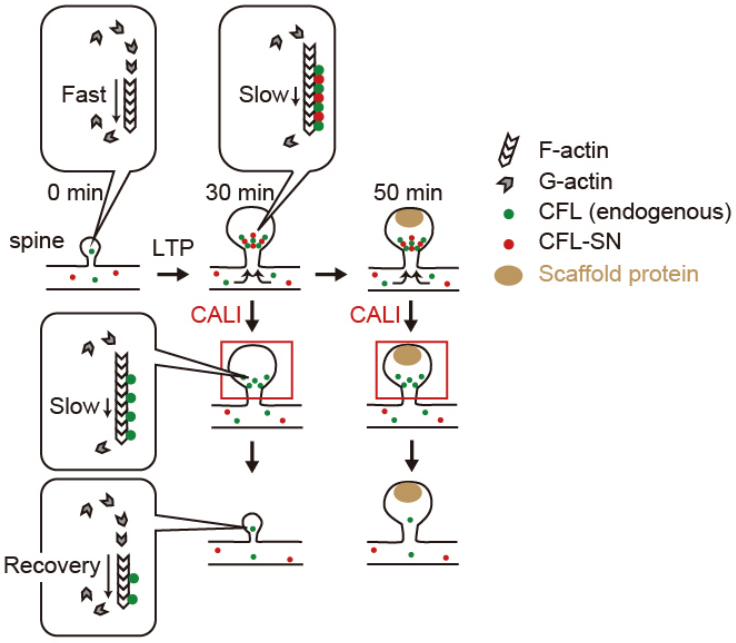

Figure S2. A molecular model for optical erasure of sLTP by CALI.
Dynamics of CFL, actin and spine structure involved in induction and erasure of sLTP. Upon induction of sLTP, CFL-SN and endogenous CFL rapidly accumulate forming a cofilactin structure in the spine, while actin turnover slows. Because of the cooperativity of the CFL molecules, CALI of CFL-SN causes a dissociation and redistribution of endogenous CFL from the dendritic spine by destabilizing the cofilactin structure, and restoring actin turnover (top). Induction of CALI 50 min after sLTP doesn't affect spine volume due to synaptic consolidation processes (bottom).

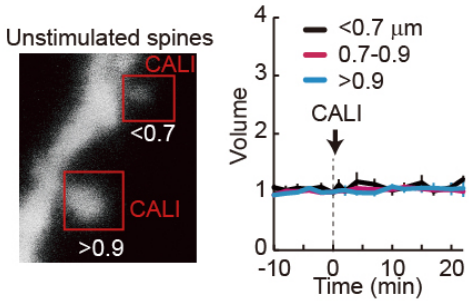

Figure S3. The effect of CALI on unstimulated spines of various sizes.
559nm laser light was illuminated on unstimulated spines of various size. Spines were classified into three groups based on size. <0.7 μm (n=12), 0.7-0.9 μm (n=12) and >0.9 μm (n=12). Spine volume (10-20 min) was statistically analyzed by a one-way ANOVA test followed by Tukey-Kramer post hoc test. $p = 0.89$.

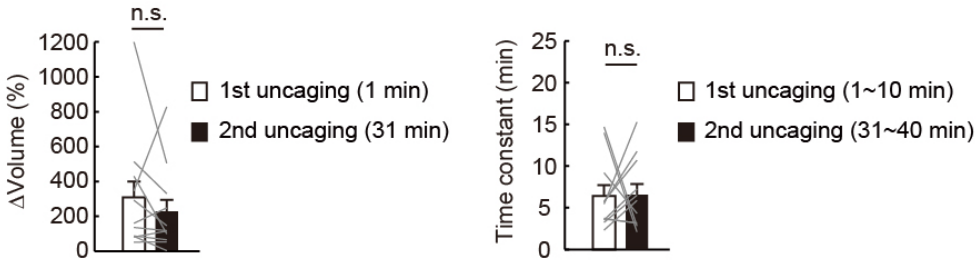

Figure S4. Comparison of volume change and decay time constant of sLTP before and after CALI.

After sLTP was induced by 1st glutamate uncaging, CALI was conducted to erase sLTP on spines expressing CFL-SN with CALI. Then LTP was induced again by the 2nd uncaging. The original data are in **Fig. 1E**.

Left: Averaged volume 1 min after 1st (before CALI) and 2nd (after CALI) uncaging. Paired t-test, p=0.38.

Right: Time constant of decay in spine volume after 1st and 2nd uncaging. Paired t-test, p=0.94.

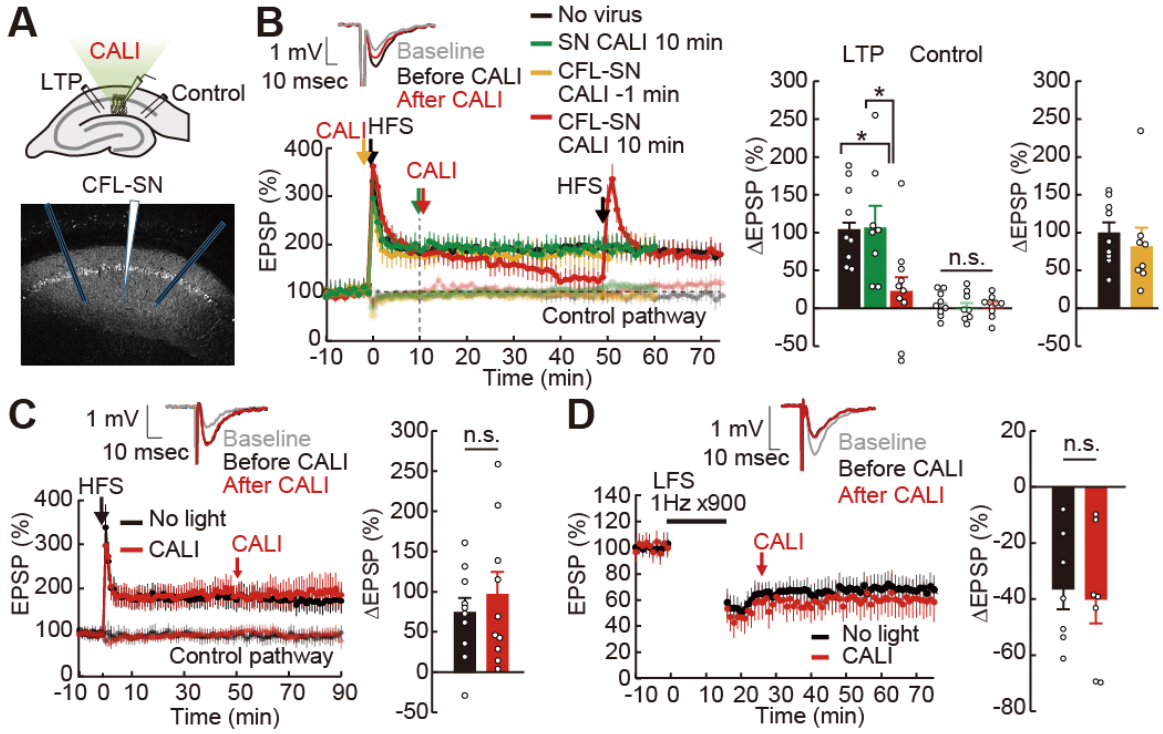

Figure S5. Optical erasure of electrically recorded LTP but not of LTD.
(**A**) fEPSPs were recorded from *stratum radiatum* of CA1 in hippocampal slices expressing CFL-SN. Light from a Hg lamp (520-550 nm band pass, 500 µW, 3 min) was used to induce CALI. A representative CFL-SN image of a slice and the positions of recording and stimulation electrodes are shown. (**B**) Effect of CALI of CFL-SN on electrically recorded LTP. Control EPSPs were recorded from mice without virus injection (n=10). CALI was induced in slices expressing CFL-SN 1 min prior to high-frequency stimulation (HFS, 100 Hz for 1sec, 3 times) (n=8), or after 10 min (n=10) or in slices expressing SN only after 10 min (n=8). Inset: examples of fEPSP traces in baseline (0 min), before CALI (10 min) and after CALI (40 min). HFS was redelivered after CALI to rule out nonspecific damage to the tissue. Bar graphs show summary in changes in fEPSP slope. Left bar graph; LTP and control pathways at 40-50 min. LTP pathway was statistically analyzed using an ANOVA test followed by Tukey-Kramer post hoc comparisons (versus CFL-SN CALI 10 min). p=0.021 (no virus), p=0.0304 (SN CALI), $F_{(2,24)}$=5.41. Control pathway was analyzed with a one-way ANOVA, p=0.88 (among 3 groups). Right bar graph; LTP pathways at 30-40 min, p=0.38 (no virus vs CFLSN CALI -1 min), Wilcoxon signed-rank test. (**C**) CALI of CFL-SN was no longer effective when it was induced 50 min after LTP induction. CALI was induced 50 min after HFS (n=10) or not induced (n=10). Bar graph (right) shows summary in changes in fEPSP slope after 30-40 min CALI. Wilcoxon signed-rank test, p=0.97. (**D**) CALI of CFL-SN did not impact LTD. EPSPs were recorded from slices expressing CFL-SN. CALI was either induced 50 min after low-frequency stimulation (LFS) (1 Hz 900 times) (n=7) or not induced (n=7). Bar graph (right) shows summary in changes in fEPSP slope after 30-40 min CALI. Wilcoxon signed-rank test, p=0.90.

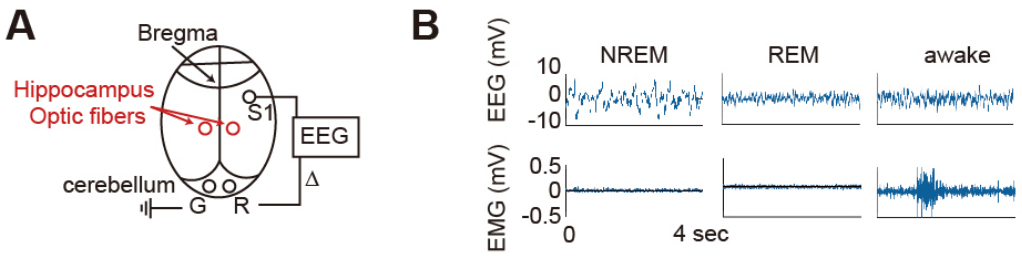

Figure S6. Online analysis of EEG and EMG for sleep state-dependent CALI.
(**A**) Locations of electrodes for EEG recording and optic fibers (red). (**B**) Representative traces of EEG and EMG judged as NREM, REM and awake.

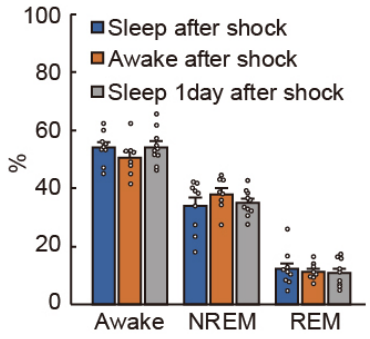

Figure S7. The effect of CALI on sleep states.
Proportion of sleep states (awake, NREM or REM) during 8 h of CALI delivery in three groups of Figure. 3D (CALI during sleep, n=9, CALI during awake, n=8, CALI during sleep 1 day after shock, n=10). CALI did not systemically alter the distributions of behavioral states. p=0.35 (awake), p=0.39 (NREM), p=0.83 (REM), one-way ANOVA respectively.

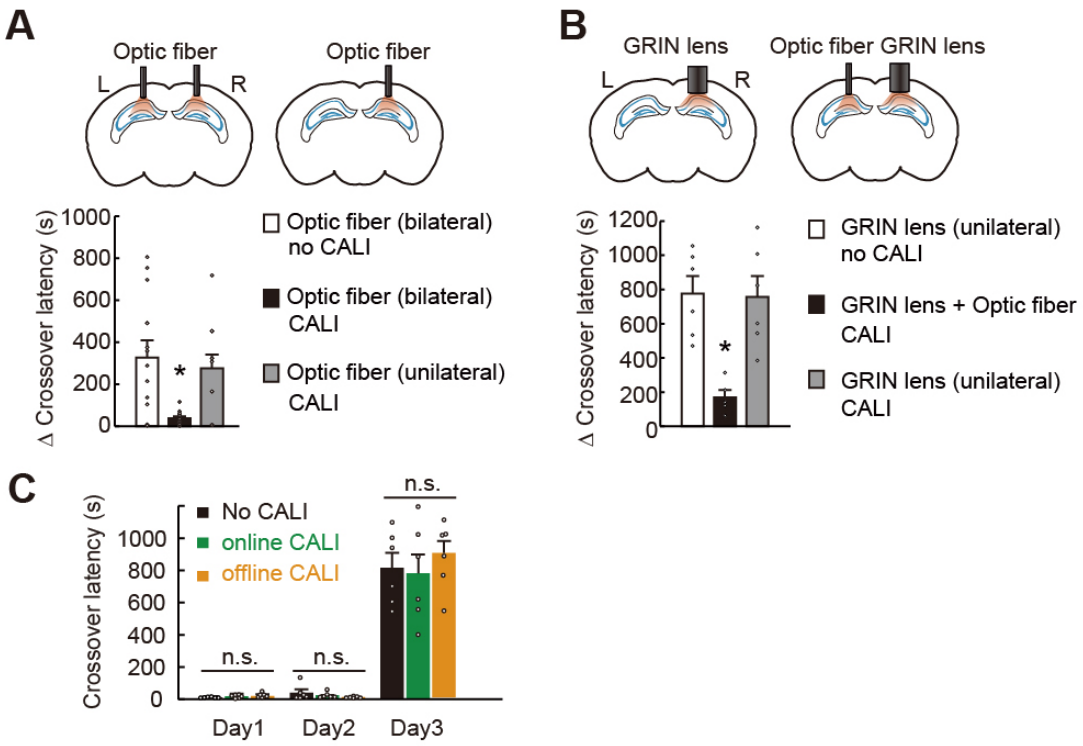

Figure S8. Unilateral CALI had no effect on IA learning.
(**A**) CALI was performed 2 min after shock either bilaterally (same as Figure. 2C) or unilaterally (n=10). One-way ANOVA test followed by Tukey-Kramer post hoc test (versus no CALI). p = 0.0022, F(2,34)=7.34. (**B**) A similar experiment but the illumination of left hemisphere was carried out through GRIN lens used for Ca^{2+}-imaging. n=6 for no CALI; n=5 for bilateral CALI; n=5 for unilateral CALI through GRIN lens. One-way ANOVA test followed by Tukey-Kramer post hoc test (versus no CALI). p = 0.0023, F(2,14)=11.12. (**C**) Averaged crossover latency of no CALI (n=6), online CALI (n=6) and offline CALI (n=6) mice in calcium imaging experiments. Significant difference among 3 groups in each day was not observed. One-way ANOVA test. p=0.12 (Day1), p=0.31 (Day2), p=0.6172.

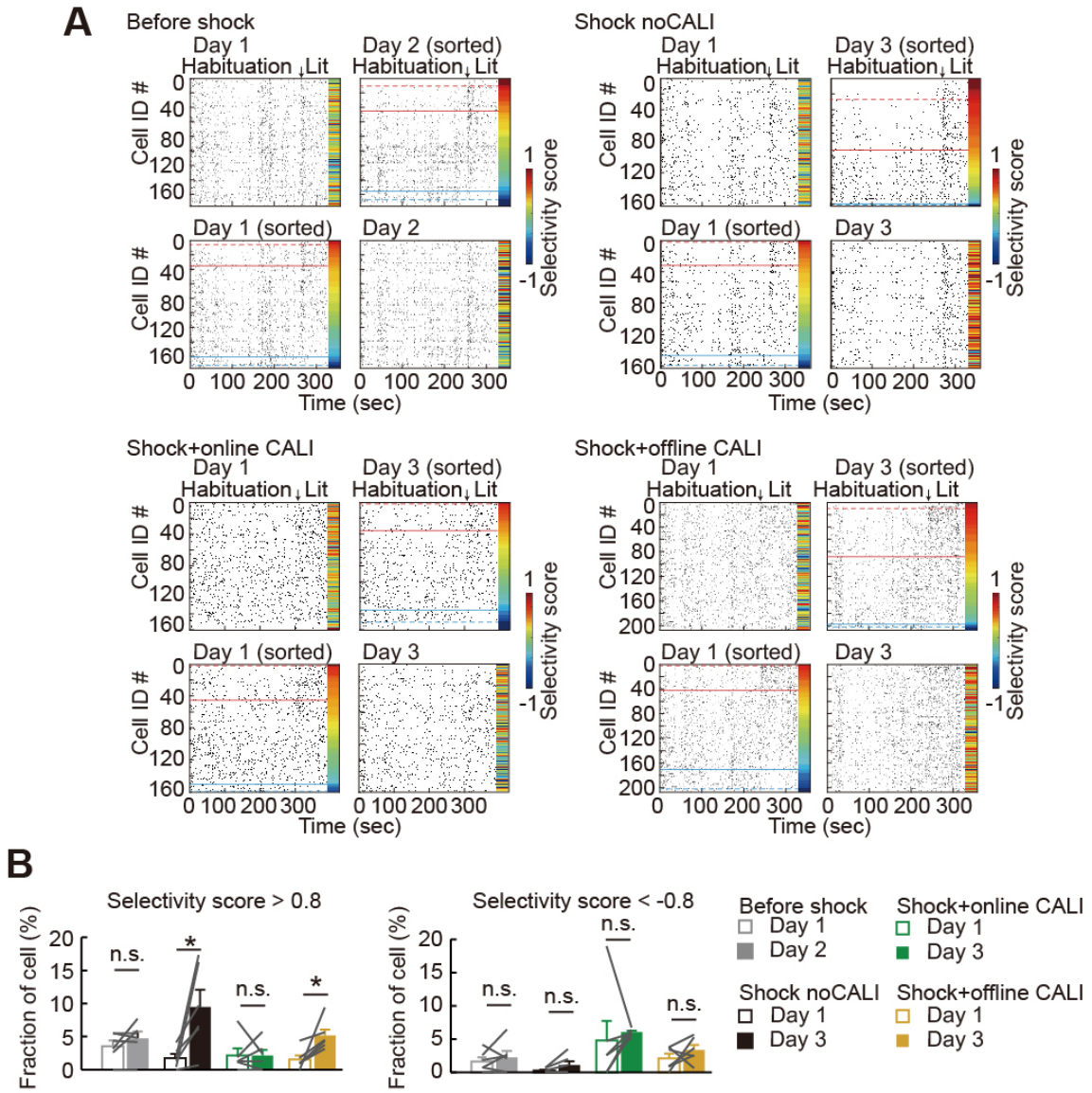

Figure S9. The effect of online and offline LTP erasure on neuronal firing selectivity. (**A**) Example data of Figure. 4C-E. Raster plot of neuronal firing in habituation chamber and IA test chamber. At time position indicated by an arrow, the mice were transferred to the lit side of the IA test chamber. Only cells that can be identified in both Day 1 and Day 3 were plotted. Top and bottom panels show the same set of neurons but sorted by the selectivity index on day 3 and day 1, respectively. Red and blue solid lines indicate selectivity score of 0.4 and -0.4 and dotted lines indicates 0.8 and -0.8. (**B**) Fraction of cells showing selectivity score >0.8 and <-0.8 respectively. All n=6. Paired t-test. Selectivity score>0.8, p= 0.25 (Before Shock), p= 0.036 (Shock no CALI), p= 0.96 (Shock+online CALI), p=0.029 (Shock+offline CALI); Selectivity score < -0.8, p= 0.50 (Before Shock), p= 0.13 (Shock noCALI), p=0.68 (Shock+online CALI), p=0.35 (Shock+offline CALI).

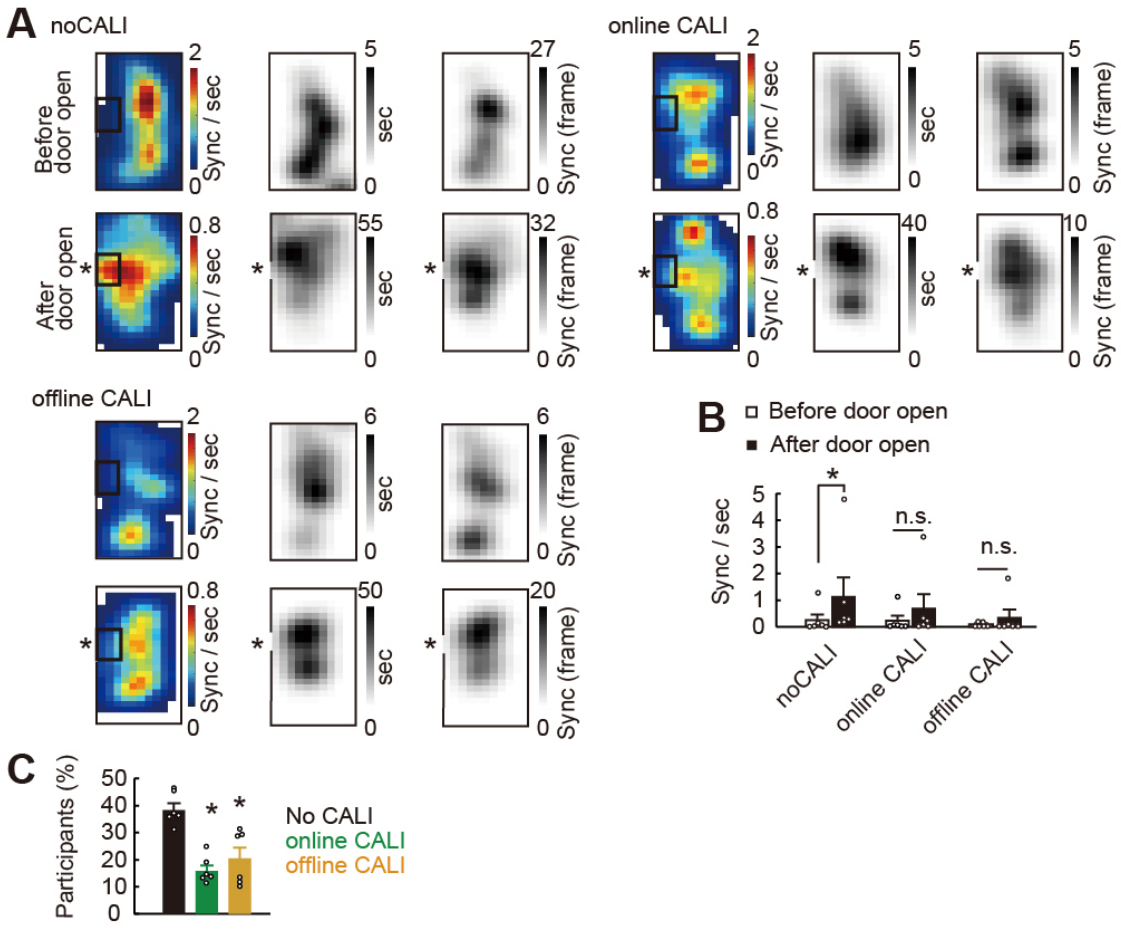

Figure S10. The effect of online and offline LTP erasure on synchronous events.
(**A**) Occupancy time and number of synchronous firing in the lit side of the IA test chamber before and after the door opens. Average of 6 animals from noCALI mice, online CALI mice and offline CALI mice are shown respectively. Raw trajectories of the animals and the position of synchronous firing are shown in Figure 4I. (**B**) Synchronous activity rate averaged from bins (4 cm x 3 cm, rectangle in the heat map) adjacent to the door from each mouse. no CALI, n=6 mice. p=0.04; Online CALI, n=6 mice. p=0.06; Offline CALI, n=6 mice. p=0.80, Wilcoxon signed-rank test. (**C**) Percentage of cells which participate in synchronous events from cells detected in both day 1 and day 3. n=6 mice, each. One-way ANOVA test followed by Tukey-Kramer post hoc test with respect to No CALI, p=0.0002 (online CALI), p=0.0019 (offline CALI), $F_{(2,15)}$=16.06.

References and Notes

1. M. Sakaguchi, Y. Hayashi, Catching the engram: Strategies to examine the memory trace. *Mol. Brain* **5**, 32 (2012). doi:10.1186/1756-6606-5-32 Medline

2. S. Tonegawa, M. D. Morrissey, T. Kitamura, The role of engram cells in the systems consolidation of memory. *Nat. Rev. Neurosci.* **19**, 485–498 (2018). doi:10.1038/s41583-018-0031-2 Medline

3. J. Z. Tsien, P. T. Huerta, S. Tonegawa, The essential role of hippocampal CA1 NMDA receptor-dependent synaptic plasticity in spatial memory. *Cell* **87**, 1327–1338 (1996). doi:10.1016/S0092-8674(00)81827-9 Medline

4. P. W. Frankland, C. O'Brien, M. Ohno, A. Kirkwood, A. J. Silva, α-CaMKII-dependent plasticity in the cortex is required for permanent memory. *Nature* **411**, 309–313 (2001). doi:10.1038/35077089 Medline

5. K. Okamoto, T. Nagai, A. Miyawaki, Y. Hayashi, Rapid and persistent modulation of actin dynamics regulates postsynaptic reorganization underlying bidirectional plasticity. *Nat. Neurosci.* **7**, 1104–1112 (2004). doi:10.1038/nn1311 Medline

6. M. Bosch, J. Castro, T. Saneyoshi, H. Matsuno, M. Sur, Y. Hayashi, Structural and molecular remodeling of dendritic spine substructures during long-term potentiation. *Neuron* **82**, 444–459 (2014). doi:10.1016/j.neuron.2014.03.021 Medline

7. E. Andrianantoandro, T. D. Pollard, Mechanism of actin filament turnover by severing and nucleation at different concentrations of ADF/cofilin. *Mol. Cell* **24**, 13–23 (2006). doi:10.1016/j.molcel.2006.08.006 Medline

8. J. R. Bamburg, A. McGough, S. Ono, Putting a new twist on actin: ADF/cofilins modulate actin dynamics. *Trends Cell Biol.* **9**, 364–370 (1999). doi:10.1016/S0962-8924(99)01619-0 Medline

9. K. Takemoto, T. Matsuda, N. Sakai, D. Fu, M. Noda, S. Uchiyama, I. Kotera, Y. Arai, M. Horiuchi, K. Fukui, T. Ayabe, F. Inagaki, H. Suzuki, T. Nagai, SuperNova, a monomeric photosensitizing fluorescent protein for chromophore-assisted light inactivation. *Sci. Rep.* **3**, 2629 (2013). doi:10.1038/srep02629 Medline

10. K. Kim, G. Lakhanpal, H. E. Lu, M. Khan, A. Suzuki, M. K. Hayashi, R. Narayanan, T. T. Luyben, T. Matsuda, T. Nagai, T. A. Blanpied, Y. Hayashi, K. Okamoto, A Temporary Gating of Actin Remodeling during Synaptic Plasticity Consists of the Interplay between the Kinase and Structural Functions of CaMKII. *Neuron* **87**, 813–826 (2015). doi:10.1016/j.neuron.2015.07.023 Medline

11. E. A. Vitriol, A. L. Wise, M. E. Berginski, J. R. Bamburg, J. Q. Zheng, Instantaneous inactivation of cofilin reveals its function of F-actin disassembly in lamellipodia. *Mol. Biol. Cell* **24**, 2238–2247 (2013). doi:10.1091/mbc.e13-03-0156 Medline

12. N. Honkura, M. Matsuzaki, J. Noguchi, G. C. Ellis-Davies, H. Kasai, The subspine organization of actin fibers regulates the structure and plasticity of dendritic spines. *Neuron* **57**, 719–729 (2008). doi:10.1016/j.neuron.2008.01.013 Medline

13. Q. Zhou, K. J. Homma, M. M. Poo, Shrinkage of dendritic spines associated with long-term depression of hippocampal synapses. *Neuron* **44**, 749–757 (2004). doi:10.1016/j.neuron.2004.11.011 Medline

14. Z. Zhou, J. Hu, M. Passafaro, W. Xie, Z. Jia, GluA2 (GluR2) regulates metabotropic glutamate receptor-dependent long-term depression through N-cadherin-dependent and cofilin-mediated actin reorganization. *J. Neurosci.* **31**, 819–833 (2011). doi:10.1523/JNEUROSCI.3869-10.2011 Medline

15. M. A. Wilson, B. L. McNaughton, Reactivation of hippocampal ensemble memories during sleep. *Science* **265**, 676–679 (1994). doi:10.1126/science.8036517 Medline

16. D. Nakayama, H. Iwata, C. Teshirogi, Y. Ikegaya, N. Matsuki, H. Nomura, Long-delayed expression of the immediate early gene Arc/Arg3.1 refines neuronal circuits to perpetuate fear memory. *J. Neurosci.* **35**, 819–830 (2015). doi:10.1523/JNEUROSCI.2525-14.2015 Medline

17. G. Girardeau, K. Benchenane, S. I. Wiener, G. Buzsáki, M. B. Zugaro, Selective suppression of hippocampal ripples impairs spatial memory. *Nat. Neurosci.* **12**, 1222–1223 (2009). doi:10.1038/nn.2384 Medline

18. L. A. Atherton, D. Dupret, J. R. Mellor, Memory trace replay: The shaping of memory consolidation by neuromodulation. *Trends Neurosci.* **38**, 560–570 (2015). doi:10.1016/j.tins.2015.07.004 Medline

19. Z. Chen, M. A. Wilson, Deciphering Neural Codes of Memory during Sleep. *Trends Neurosci.* **40**, 260–275 (2017). doi:10.1016/j.tins.2017.03.005 Medline

20. K. Ghandour, N. Ohkawa, C. C. A. Fung, H. Asai, Y. Saitoh, T. Takekawa, R. Okubo-Suzuki, S. Soya, H. Nishizono, M. Matsuo, M. Osanai, M. Sato, M. Ohkura, J. Nakai, Y. Hayashi, T. Sakurai, T. Kitamura, T. Fukai, K. Inokuchi, Orchestrated ensemble activities constitute a hippocampal memory engram. *Nat. Commun.* **10**, 2637 (2019). doi:10.1038/s41467-019-10683-2 Medline

21. D. Miyamoto, D. Hirai, C. C. A. Fung, A. Inutsuka, M. Odagawa, T. Suzuki, R. Boehringer, C. Adaikkan, C. Matsubara, N. Matsuki, T. Fukai, T. J. McHugh, A. Yamanaka, M. Murayama, Top-down cortical input during NREM sleep consolidates perceptual memory. *Science* **352**, 1315–1318 (2016). doi:10.1126/science.aaf0902 Medline

22. Y. Ziv, L. D. Burns, E. D. Cocker, E. O. Hamel, K. K. Ghosh, L. J. Kitch, A. El Gamal, M. J. Schnitzer, Long-term dynamics of CA1 hippocampal place codes. *Nat. Neurosci.* **16**, 264–266 (2013). doi:10.1038/nn.3329 Medline

23. P. Rajasethupathy, S. Sankaran, J. H. Marshel, C. K. Kim, E. Ferenczi, S. Y. Lee, A. Berndt, C. Ramakrishnan, A. Jaffe, M. Lo, C. Liston, K. Deisseroth, Projections from neocortex mediate top-down control of memory retrieval. *Nature* **526**, 653–659 (2015). doi:10.1038/nature15389 Medline

24. B. Bontempi, C. Laurent-Demir, C. Destrade, R. Jaffard, Time-dependent reorganization of brain circuitry underlying long-term memory storage. *Nature* **400**, 671–675 (1999). doi:10.1038/23270 Medline

25. P. W. Frankland, B. Bontempi, L. E. Talton, L. Kaczmarek, A. J. Silva, The involvement of the anterior cingulate cortex in remote contextual fear memory. *Science* **304**, 881–883 (2004). doi:10.1126/science.1094804 Medline

26. Y. Zhang, H. Fukushima, S. Kida, Induction and requirement of gene expression in the anterior cingulate cortex and medial prefrontal cortex for the consolidation of inhibitory avoidance memory. *Mol. Brain* **4**, 4 (2011). doi:10.1186/1756-6606-4-4 Medline

27. G. Riedel, J. Micheau, A. G. M. Lam, E. L. Roloff, S. J. Martin, H. Bridge, L. de Hoz, B. Poeschel, J. McCulloch, R. G. M. Morris, Reversible neural inactivation reveals hippocampal participation in several memory processes. *Nat. Neurosci.* **2**, 898–905 (1999). doi:10.1038/13202 Medline

28. E. Shimizu, Y. P. Tang, C. Rampon, J. Z. Tsien, NMDA receptor-dependent synaptic reinforcement as a crucial process for memory consolidation. *Science* **290**, 1170–1174 (2000). doi:10.1126/science.290.5494.1170 Medline

29. A. Hayashi-Takagi, S. Yagishita, M. Nakamura, F. Shirai, Y. I. Wu, A. L. Loshbaugh, B. Kuhlman, K. M. Hahn, H. Kasai, Labelling and optical erasure of synaptic memory traces in the motor cortex. *Nature* **525**, 333–338 (2015). doi:10.1038/nature15257 Medline

30. H. Murakoshi, H. Wang, R. Yasuda, Local, persistent activation of Rho GTPases during plasticity of single dendritic spines. *Nature* **472**, 100–104 (2011). doi:10.1038/nature09823 Medline

31. K. Takemoto, H. Iwanari, H. Tada, K. Suyama, A. Sano, T. Nagai, T. Hamakubo, T. Takahashi, Optical inactivation of synaptic AMPA receptors erases fear memory. *Nat. Biotechnol.* **35**, 38–47 (2017). doi:10.1038/nbt.3710 Medline

32. K. Z. Tanaka, H. He, A. Tomar, K. Niisato, A. J. Y. Huang, T. J. McHugh, The hippocampal engram maps experience but not place. *Science* **361**, 392–397 (2018). doi:10.1126/science.aat5397 Medline

33. T. Kitamura, S. K. Ogawa, D. S. Roy, T. Okuyama, M. D. Morrissey, L. M. Smith, R. L. Redondo, S. Tonegawa, Engrams and circuits crucial for systems consolidation of a memory. *Science* **356**, 73–78 (2017). doi:10.1126/science.aam6808 Medline

34. G. Vetere, L. Restivo, C. J. Cole, P. J. Ross, M. Ammassari-Teule, S. A. Josselyn, P. W. Frankland, Spine growth in the anterior cingulate cortex is necessary for the consolidation of contextual fear memory. *Proc. Natl. Acad. Sci. U.S.A.* **108**, 8456–8460 (2011). doi:10.1073/pnas.1016275108 Medline

35. K. Takehara-Nishiuchi, Prefrontal-hippocampal interaction during the encoding of new memories. *Brain Neurosci. Adv.* **4**, 2398212820925580 (2020). doi:10.1177/2398212820925580 Medline

36. N. Maingret, G. Girardeau, R. Todorova, M. Goutierre, M. Zugaro, Hippocampo-cortical coupling mediates memory consolidation during sleep. *Nat. Neurosci.* **19**, 959–964 (2016). doi:10.1038/nn.4304 Medline

37. F. Xia, B. A. Richards, M. M. Tran, S. A. Josselyn, K. Takehara-Nishiuchi, P. W. Frankland, Parvalbumin-positive interneurons mediate neocortical-hippocampal interactions that are necessary for memory consolidation. *eLife* **6**, e27868 (2017). doi:10.7554/eLife.27868 Medline

38. Y. D. Riani, T. Matsuda, K. Takemoto, T. Nagai, Green monomeric photosensitizing fluorescent protein for photo-inducible protein inactivation and cell ablation. *BMC Biol.* **16**, 50 (2018). doi:10.1186/s12915-018-0514-7 Medline

39. J. C. Grieger, V. W. Choi, R. J. Samulski, Production and characterization of adeno-associated viral vectors. *Nat. Protoc.* **1**, 1412–1428 (2006). doi:10.1038/nprot.2006.207 Medline

40. A. Bota, A. Goto, S. Tsukamoto, A. Schmidt, F. Wolf, A. Luchetti, J. Nakai, H. Hirase, Y. Hayashi, Shared and unique properties of place cells in anterior cingulate cortex and hippocampus. *bioRxiv* 2021.03.29.437441 [Preprint] (2021); doi.org/10.1101/2021.03.29.437441